Nuclear Instruments and Methods in Physics Research A 624 (2010) 255–259

Contents lists available at ScienceDirect

Nuclear Instruments and Methods in Physics Research A

journal homepage: www.elsevier.com/locate/nima

2-D response mapping of multi-linear silicon drift detectors

A. Castoldi [a,b,*], C. Guazzoni [a,b], R. Hartmann [c], D. Mezza [a,b], L. Strüder [e,d,f], F. Tassan Garofolo [a,b]

[a] Politecnico di Milano, Dip. Elettronica e Informazione, Piazza L. da Vinci 32, 20133 Milano, Italy
[b] INFN, Sezione di Milano, Via Celoria 16, 20133 Milano, Italy
[c] PNSensor GmbH, Römerstrasse 28, 80803 München, Germany
[d] MPI Halbleiterlabor, Otto-Hahn-Ring 6, 81739 München, Germany
[e] Max-Planck Institut für extraterrestrische Physik, Giessenbachstrasse, 85741 Garching, Germany
[f] Universität Siegen, FB Physik, Emmy-Noether Campus, Walter Flex Strasse 3, 57068 Siegen, Germany

ARTICLE INFO

Available online 8 June 2010

Keywords:
X-ray imaging
X-ray spectroscopy
Position-sensitive detectors
Silicon drift detectors

ABSTRACT

Multi-linear silicon drift detectors (MLSDDs) are good candidates to fulfill simultaneous requirements for 2-D position-sensing and spectroscopy applications. The optimization of their design and performance as 2-D imagers requires a detailed study of timing properties of the charge cloud in the MLSDD architecture. In particular it is important to experimentally determine the dependence of the measured amplitude and time-of-arrival on the photon position of interaction so as to derive the 2D detector response. In this paper we will present a detailed experimental characterization aimed at measuring the detector amplitude response and its timing response. The dependence of charge cloud drift time on precise position of interaction has been measured as a function of detector biasing conditions.

1. Introduction

Multi-linear silicon drift detectors [1–4] (hereafter MLSDDs) were proposed in 1996 as an evolution of multi-anode silicon drift detectors to improve spectroscopy performance and event rate [5] in the detection of X-rays and ionizing particles. They are silicon drift detectors in which signal electrons are confined within parallel drifting columns (or channels) by means of a suitable, that is the time interval combination of deep p and n implants at a few micrometers from the front surface. An electrostatic field is responsible for the transport of signal charges toward point-like anodes in times of the order of a few microseconds for a drift length of 1 cm. The measure of the drift time, that is the time interval between radiation interaction and the arrival of signal charge at the collecting electrode, provides the position of interaction, while the orthogonal coordinate is provided by the granularity of the collecting anodes. Moreover the deposited energy can be measured with spectroscopic resolution with moderate Peltier cooling, thanks to point-like anodes of very low capacitance (<100 fF) via on-chip JFETs [6].

Fig. 1 shows a scheme of principle of the MLSDD prototype used in the present tests. The starting material is a detector-grade high-resistivity n-doped silicon substrate (450 μm thick). The detector volume is fully depleted to ensure high detection efficiency. A segmented shallow p+ implant on the back side acts as entrance window for the radiation. An array of p+ strips is implanted on the front side (anode side) and is biased by means of an integrated resistive voltage divider. An array of deep p implants (channel stops) defines the border between adjacent drifting channels. An array of deep n-implants (channel guides) located in the center of each drifting channel has the twofold effect of increasing the potential barriers along the lateral direction (i.e. perpendicular to the drift) and therefore of improving charge confinement and of enhancing electron drift velocity [7]. The electrons' drift takes place within a high-energy n-type implant located a few micrometers away from the finely structured front surface.

Signal electrons, generated at a given detector depth (depending on the type of incident particles), are focused by the component of the electric field, directed along the detector depth (z), henceforth called depletion field, toward the detector front surface, until they reach one of the drifting channels. While being focused on the drift channel the signal electrons drift toward the anode owing to the field component along the y direction, henceforth called the drift field. Signal holes are immediately collected by the p+ strip closest to the interaction point.

At a first level of approximation the electron cloud spread along x and y directions is approximately isotropic during the initial motion across the thickness toward the drift channels (henceforth called focusing). This initial broadening process lasts a few tens of nanoseconds and stops when the signal electrons

* Corresponding author at: Politecnico di Milano, Dip. Elettronica e Informazione, Piazza L. da Vinci 32, 20133 Milano, Italy. Tel.: +39 02 2399 6321; fax: +39 02 2399 6309.
E-mail address: Andrea.Castoldi@polimi.it (A. Castoldi).

0168-9002/$ - see front matter © 2010 Elsevier B.V. All rights reserved.
doi:10.1016/j.nima.2010.05.059

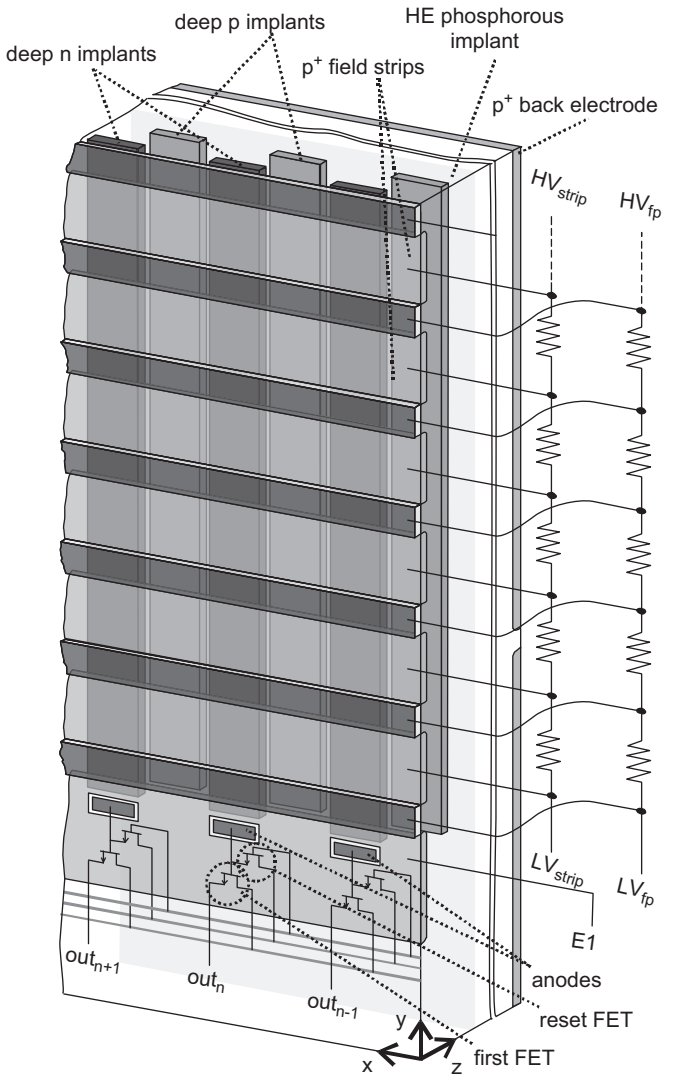

Fig. 1. Sketch of the architecture of the MLSDD prototype used in the present tests.

reach the drift channels. At low levels of charge injection (when electrostatic repulsion is negligible) the charge cloud expansion, during the focusing process, is dominated by thermal diffusion. At higher levels of charge injection, a further and often dominant contribution to charge broadening arises from electrostatic repulsion. Once the focusing process is terminated, the charge distribution is then "frozen" into the drift channels and electrons are transported to the readout anodes without further broadening in the lateral (x) direction, irrespective of the drifted distance, due to the lateral potential barriers. Only longitudinal (i.e. along the y direction) broadening continues to increase while electrons move inside the drift channel.

The previously highlighted features of MLSDDs make them suitable for 2-D position sensing with position resolution independent of the interaction point. Moreover, the suppression of lateral diffusion improves the capability to handle multi-hit events and the maximum processing rate with respect to conventional multi-anode drift detectors, which require a cluster separation algorithm at high particle occupancy [10]. A careful optimization of drift channel pitch opens the way also to spectroscopy applications and to high position resolution.

However the optimization of their design and performance as 2-D imagers requires a detailed study of timing properties of the charge cloud moving in the complex electric field distribution that characterizes the MLSDD architecture. In particular it is important to experimentally determine the 2D detector response over the active area.

In this paper we will present a detailed experimental characterization aimed at mapping the detector amplitude and timing response. Section 2 describes the experimental setup and the characterization method. Section 3 reports the main results of the amplitude and drift time mapping. Section 4 evaluates the dependence of drift time on interaction coordinate as a function of detector biasing conditions and of the charge injection level.

2. Experimental setup and method

In order to measure the 2-D response matrix of the detector the use of a pulsed infrared laser to simulate the effects of X-ray ionization or of single ionizing particles makes things easier, thanks to its intrinsic capability of accuracy in beam positioning and in time synchronization.

We have developed an advanced IR laser-based test suite featuring an x–y stage system for mechanical movement with micrometer positioning capabilities (repeatability of positioning better than 1 μm), and an optical axis that allows beam splitting in order to both focus the IR laser pulse and visualize the laser spot on the detector surface with a video camera. Fig. 2 shows the block diagram of the measurement setup and of the readout electronics. Each detector output channel is preamplified and shaped by the analog front-end (5 poles pseudo-Gaussian shaper with 250 ns shaping time constant), which delivers a unipolar signal and a bipolar signal, which are then digitized by a Tektronix TDS 540D digital oscilloscope. The maximum of the unipolar shaper signal provides information on amplitude of the collected signal, which indicates the amount of deposited charge, while the zero-crossing time of the bipolar signal provides arrival time of the signal charge. The controller (Newport MM4006) of the micrometer stages and the digital oscilloscope are connected via GPIB bus to the host PC, which acquires the digitized waveforms. A LabView code allows defining the stepping sequence (which can also correct for small misalignment of the x–y stages with respect to the detector axes) and setting the parameters for the digital filtering algorithm, which computes pulse amplitude and pulse arrival time. The laser driving system (PicoQuant PDL 800-D) allows for repetition rates up to 80 MHz, with pulse width <100 ps (70–90 ps FWHM as a function of intensity level). The wavelength of the selected laser head is 905 nm (± 10 nm), which assures an absorption length in silicon of about 30 μm at room temperature. The laser intensity can be adjusted to deliver pulses with energy up to 40 pJ, which is well suited to simulate a wide dynamic range of intensities. The laser output is then launched into a single-mode optical fiber with core/cladding diameter 6/125 μm coupled to one eye-piece slot of a microscope. A 20 × objective with ultra-long working distance is used to focus the laser spot on the detector surface.

The MLSDD prototype used in the present measurement campaign features a linear geometry with 1.1 cm drift length and 200 μm drift channel width, and its design was optimized also for operation at high drift fields [8].

In order to determine the laser spot size a direct measurement has been carried out using the fine aluminum pattern present on the anode side of one prototype of MLSDD. In particular profiting of the different reflective properties of the aluminum strips on the detector surface with respect to the strips implanted in naked silicon, it was possible to acquire the output voltage at one of the drift channels of the detector while moving the laser source in 1 μm steps along the drift direction. Fig. 3 shows the corresponding measured amplitude signal. As can be noticed, there

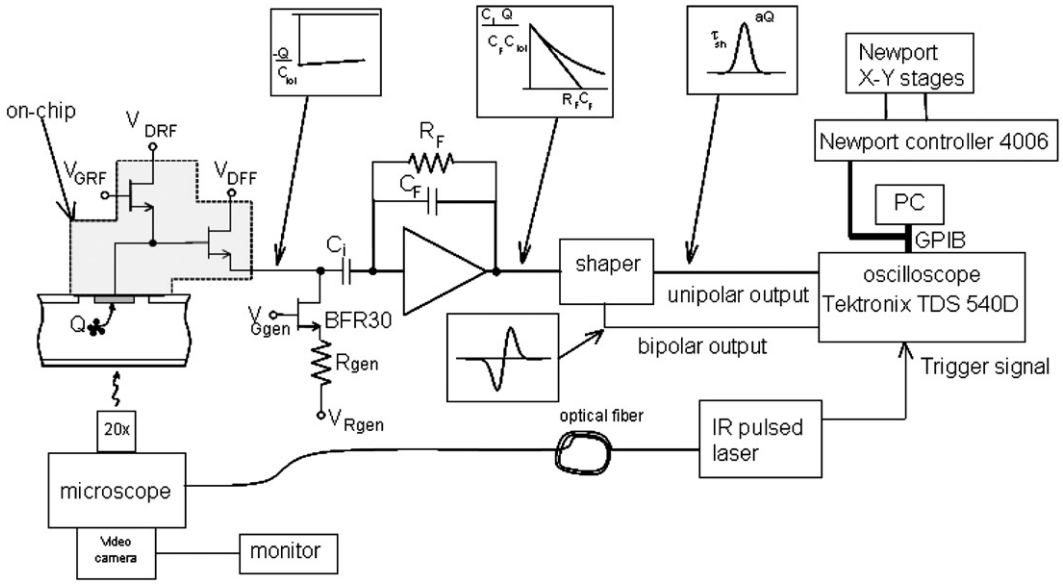

Fig. 2. Block diagram of the measurement setup and of the readout electronics.

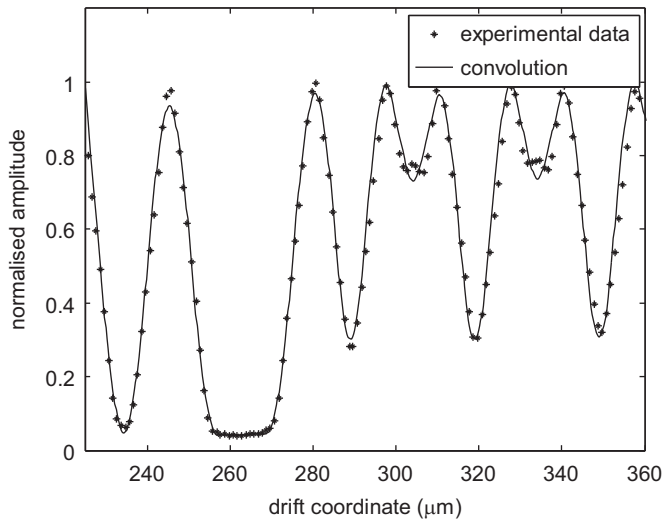

Fig. 3. Result of the convolution of the profile of the laser spot along the drift coordinate with the transmittance pattern compared with the experimental data.

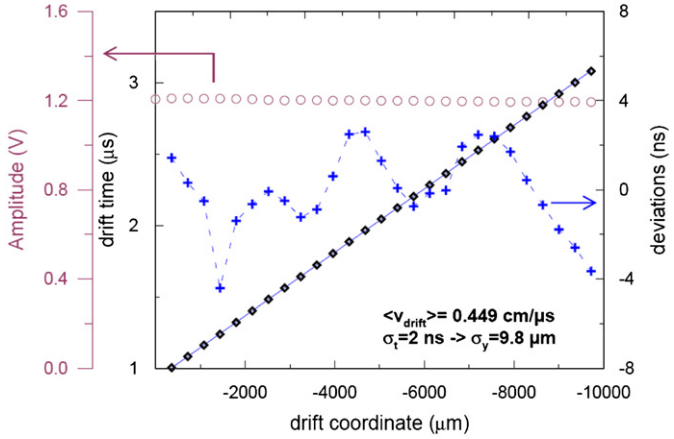

Fig. 4. Drift time as a function of laser spot incidence position in the center of the channel at 400 V/cm applied drift field and 300 K detector temperature (diamonds). The solid line is the linear fit. The deviations from the linear fit (crosses, right axis) and the measured amplitudes (circles, second left axis) are also shown.

is a considerable voltage swing corresponding to the different incident points as a result of the aluminum surface pattern and of the laser spot profile. In order to get a quantitative evaluation of the laser spot profile from the experimental measurements we assumed that the detector surface covered by a metal layer has negligible transmittance for the infrared laser, while the naked silicon area has unitary transmittance. From the analysis of the measured data shown in Fig. 3 we assumed a trapezoidal profile with sharp edges for the optical power distribution and we deconvoluted the modeled surface transmittance from the measured intensity pattern. The resulting FWHM of the laser spot is 11 μm diameter, well suited as a fine probe for detector characterization.

Fig. 4 shows the drift time as a function of laser spot position in the center of the channel at 400 V/cm applied drift field and 300 K detector temperature. The average drift velocity derived from the linear fit is 0.449 cm/μs. The transport velocity is very uniform over the whole drift length; the time deviations from the linear fit are in the order of 2 ns rms, corresponding to 10 μm rms in position.

The detector amplitude and timing response have been obtained with a fine scan of the detector surface (exposing the p+ strips of the back side to the laser beam) with 10 μm × 10 μm steps. At each scan position the pulse amplitude and charge drift time were measured.

3. 2-D mapping of the amplitude and of the drift time response

The laser intensity was set such that the charge injection level was 21,000 electrons.

3.1. Amplitude mapping

Fig. 5 shows the map of the measured amplitude. As is clearly visible, the amplitude is constant over the whole drift channel width. The standard deviation of the measured amplitudes in the central area is 0.35%. The amplitude drops to 50% at the rim of the drift channel on the middle of the deep p implant, which defines the drift channel width.

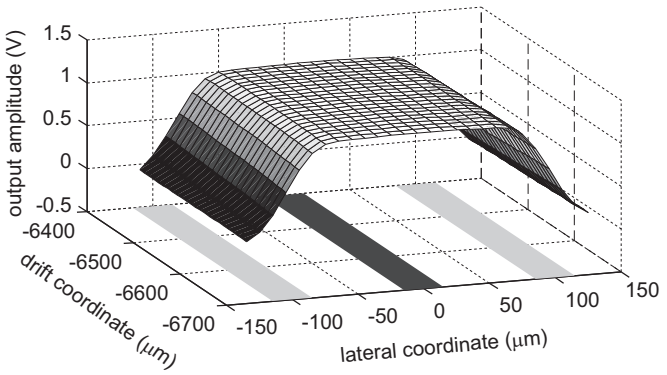

Fig. 5. 2-D amplitude response of the detector. One drift channel is shown.

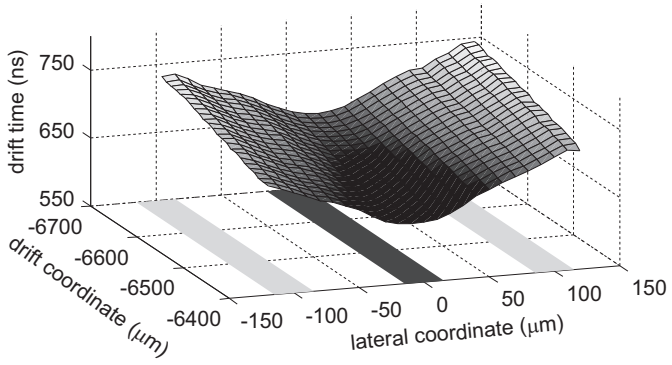

Fig. 6. 2-D drift time response of the detector. One drift channel is shown.

3.2. Drift time mapping

The most interesting result is the map of drift time, shown in Fig. 6. As can be noticed, the 2D distribution of drift times is strictly correlated to the confining potential/channel guide generated by the deep implants. The drift time related to photons interacting in the channel-stop area is longer than the one of photons incident on the channel-guide area. This has a clear impact on the achievable position resolution.

3.3. Discussion

In order to better understand the result shown in Fig. 6 we model the drift field (i.e. the electric field component along the drift direction, y) experienced by the charge cloud during its motion as

$$E_y(x,\ y,\ z) = E_d + \Delta E_y(x,\ y,\ z) \tag{1}$$

where E_d is the nominal applied drift field (which does not depend on the spatial coordinates) and ΔE_y is a sinusoidal-like perturbation term that originates mainly from the segmentation of the field electrodes and, generally to a lesser extent, from the bias non-linearity. The pattern of deep implants introduces an additional source of spatial dependence of the perturbation field. As we have shown in Refs. [1,7] the effect of the deep p implant is to locally increase the surface potential where the deep implanted region is located (i.e. increase the perturbation field caused by the segmentation of the field strips). The effect of the deep n implant is to smoothen the potential in the drift direction underneath where the deep n-implants are located.

In this way the perturbation field has a minimum on the middle of the drift channel and a maximum on the middle of the channel-stop area, at the edge of each drift channel. Finally, the field perturbation decreases with depth, z, as surface effects are attenuated.

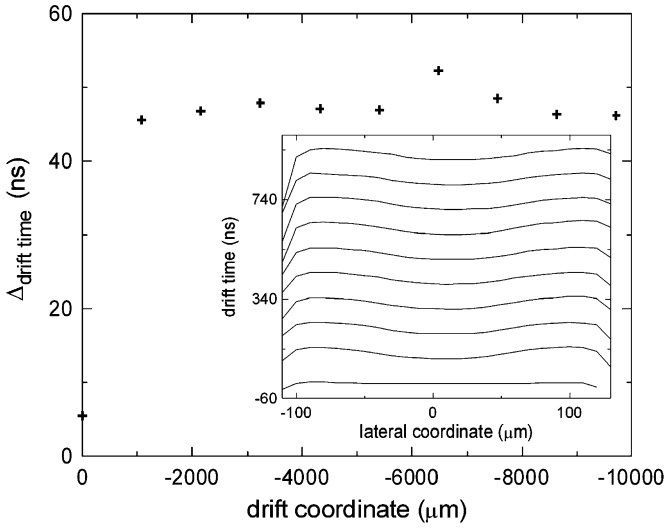

Fig. 7. Difference of drift times of the photons incident on the middle of the channel stop and on the middle of the channel as a function of drift coordinate. The inset shows the dependence of drift time on lateral coordinate (x) for different drift distances spaced 1.08 mm starting from the point 46 μm away from the anode center. Back voltage is 150 V.

The drift time depends on the drift field as

$$T_d(x,\ y,\ z) = \int_\Gamma \frac{dx}{\mu_n E_y(x,\ y,\ z)} \tag{2}$$

and directly reflects the shape of the perturbation field and of the confining potential. If we compute the difference of the drift time of the photons incident on the middle of the channel stop (i.e. edge of a drift channel) and the one of those incident on the middle of the channel we find that the time difference stays nearly constant and is about 47 ns, as shown in Fig. 7. At the applied drift field this has a significant impact of about 0.2 mm on position resolution. The first incidence point, located very close to the anode, shows on the contrary a negligible variation of drift time across the drift channel. This is explained as the electrons traverse the silicon thickness and are directly collected by the anodes without being focused on the drift channel.

4. Effect of back voltage and charge injection level

We have repeated the same measurements discussed in Section 3 for different values of the back side voltage and at different charge injection levels up to 340,000 electrons. Fig. 8 shows the measured dependence of drift time on lateral coordinate at 4.366 mm from the anode center for different levels of charge injection and with the back side biased at −150 V. As is evident in the figure, at lower levels of charge injection—when the charge cloud's lateral spread is limited [9] and is smaller than the width of the deep n-implanted region—the full charge distribution drifts within the deep n-implanted region even if the laser spot impinges out of the center of the drift channel (and, hence, of the deep n-implant). At increasing levels of charge injection the lateral spread of the charge cloud traversing the detector depth increases and the dependence of the drift time on lateral injection position within the deep n-implanted area becomes visible. A second interesting point is the fact that the maximum deviation of drift time occurs at lateral positions outside the rim of the drift

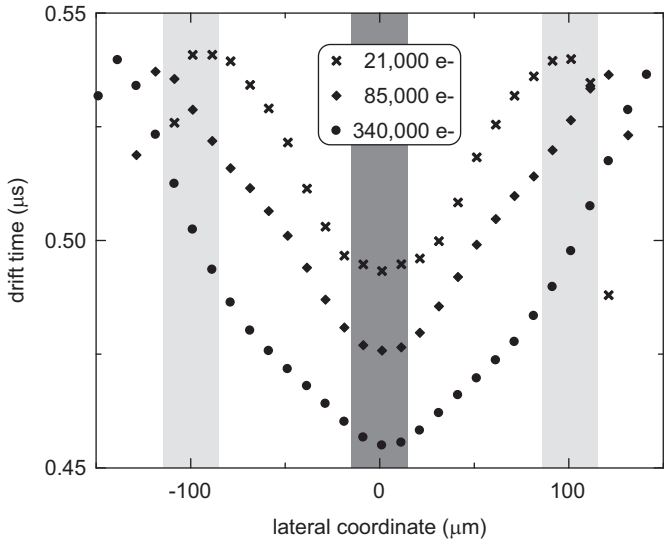

Fig. 8. Measured dependences of drift times on lateral coordinate at 4.366 mm away from the anode center for different levels of charge injection. The dark-gray filled areas indicate the deep n-implants while the light-gray filled areas indicate the deep p-implants.

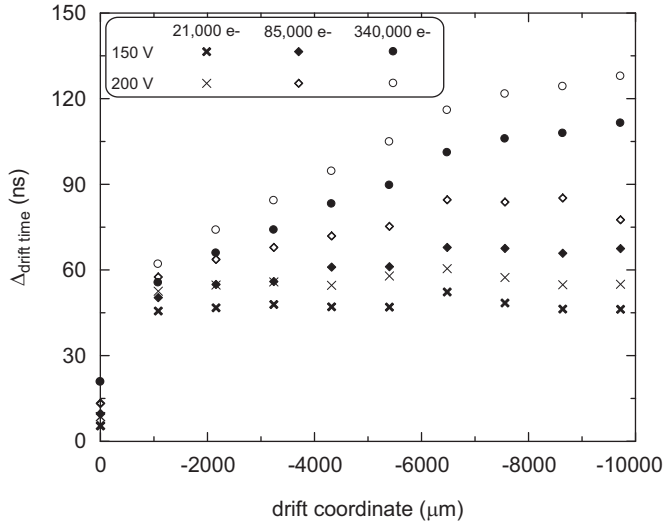

Fig. 9. Differences of drift times of the photons incident on the middle of the channel-stop and the one of those incident on the middle of the channel as a function of drift coordinate for two back voltages and three levels of charge injection as reported in the legend.

channel. An additional effect is the reduction of the drift times, as a result of the charge density of the electron cloud that smooths the potential perturbations.

Fig. 9 shows the differences of drift times of the photons incident on the middle of the channel stop and of those incident on the middle of the channel as a function of drift coordinate for two back voltages and three levels of charge injection. At higher back voltages the dependence of drift time on lateral position is more significant. This can be explained by taking into account the actual trajectory of the charge cloud in reaching the drifting channel. At lower back voltages the time spent by the electrons at depths where the effect of the deep implanted regions is negligible is longer and therefore the time difference caused by the deep implanted regions is less visible. At higher levels of charge injection there is an increasing dependence of drift time difference on drift coordinate. A possible interpretation can be suggested again with the help of the actual electron cloud trajectory. At higher levels of charge injection the spread of the charge cloud is larger due to Coulomb repulsion and part of the charge is collected even when the lateral injection point is into the neighboring channel but with a slower focusing to the channel center.

5. Outlook

In this paper we presented the results of a detailed mapping of amplitude and drift time response of a prototype of a multi-linear silicon drift detector as a function of different biasing conditions of the detector and at different levels of charge injection. This experimental characterization, besides providing a deeper understanding in the transport properties of MLSDD, offers a detailed data-set useful to predict the detector response as a function of operating conditions and design properties and to be used for comparison with device simulations.

In the near future the impact of operating temperature on the detector response will be experimentally evaluated as well as the impact of a higher level of charge injection.

Acknowledgments

The authors thank P. Holl, F. Schopper and the technology staff of the MPI Halbleiterlabor and of PNSensor GmbH in Munich for the continuous support in technology development and detector production. The perfect bonding of all the detector prototypes by S. Masci is deeply acknowledged.

This work was supported by Istituto Nazionale di Fisica Nucleare (INFN) within the framework of RIXFEL (study and development of high-speed X-ray imaging detectors for the future Free Electron Laser facilities) experiment.

References

[1] A. Castoldi, P. Rehak, P. Holl, Nucl. Instr. and Meth. A 377 (1996) 375.
[2] A. Castoldi, P. Rehak, P. Holl, IEEE Trans. Nucl. Sci. NS-44 (1997) 134.
[3] A. Castoldi, A. Galimberti, C. Guazzoni, P. Rehak, R. Hartmann, L. Strüder, Nucl. Instr. and Meth. A 568 (2006) 89.
[4] A. Castoldi, A. Galimberti, E. Gatti, C. Guazzoni, P. Rehak, L. Strüder, IEEE Trans. Nucl. Sci. NS-53 (2006) 601.
[5] P. Rehak, et al., Nucl. Instr. and Meth. A 235 (1985) 224.
[6] V. Radeka, et al., IEEE Electron Device Lett. ED-10 (1989) 91.
[7] A. Castoldi, C. Guazzoni, L. Strüder, IEEE Trans. Nucl. Sci. NS-49 (2002) 1055.
[8] A. Castoldi, C. Guazzoni, R. Hartmann L. Strüder, Optimized design topologies for position-sensitive silicon drift detectors operating at high drift fields, in: Nuclear Science Symposium Conference Record, 2008, IEEE, 19–25 October 2008, Dresden, Germany.
[9] A. Castoldi, C. Guazzoni, R. Hartmann, P. Madoglio, L. Strüder, IEEE Trans. Nucl. Sci. NS-56 (2) (2009) 496.
[10] V. Petracek, Czech. J. Phys. 48/S1 (1998) 87–96.